Check for updates

LIMNOLOGY
and
OCEANOGRAPHY: METHODS

ASLO

Limnol. Oceanogr.: Methods 2025
© 2025 Association for the Sciences of Limnology and Oceanography.
doi: 10.1002/lom3.10676

NEW METHODS

Fractionation of ultrafine particles from marine sediment for organic geochemical measurement

Guangjin Zheng,[1,2] **Mengyao Shen**,[1,2] **Nan Wang**,[3] **Yangli Che**,[1,2] **Haoshuai Li**,[1,2] **Caiqing Yan**,[4] **Rui Bao**[1,2]*

[1]Frontiers Science Center for Deep Ocean Multispheres and Earth System, Key Laboratory of Marine Chemistry Theory and Technology, Ministry of Education, Ocean University of China, Qingdao, China; [2]Laboratory for Marine Geology, Qingdao Marine Science and Technology Center, Qingdao, China; [3]Key Lab of Submarine Geosciences and Prospecting Techniques, Ministry of Education, Ocean University of China, Qingdao, China; [4]Qingdao Key Laboratory for Prevention and Control of Atmospheric Pollution in Coastal Cities, Environment Research Institute, Shandong University, Qingdao, China

Abstract

In traditional grain-size separation of marine sediment using the sieve technique, the majority of organic matter (OM) in the ultrafine sediment is yet hardly further separated. In this study, we suggest an inertial sieving method that utilizes an ultrafine particle separator (UPS), which consists of a suspended particle generator (SPG) combined with a particle size separating device (PSSD), to separate ultrafine particles from marine sediments. Specifically, our method can fractionate ultrafine particles (< 10 μm) into eight different grain size categories: 0.43–0.65, 0.65–1.10, 1.10–2.10, 2.10–3.30, 3.30–4.70, 4.70–5.80, 5.80–9.00, and 9.00–10.00 μm. We evaluate the effectiveness of this method in fractionating ultrafine marine sediment from the China Marginal Sea. Our study find that the inertial sieving method achieved a high mass recovery rate of 77.7–88.7% and a sieving accuracy of 75–94% for sediment samples. Additionally, we measure total organic carbon (OC) and stable carbon isotopes of OM associated with these eight ultrafine sediments. Overall, we suggest that the inertial sieving method has a high potential to effectively fractionate the marine sediments with particle sizes below 10 μm for further organic geochemical analysis on these grain size fractionated sediments.

Preservation of organic carbon (OC) in sediments plays a key role in the global carbon cycle (Arnarson and Keil 2007). In order to explore the burial mechanisms of marine sediment OM, the processes regulating the distribution and preservation of OC in marine sediments need to be better characterized (Coppola et al. 2007; LaRowe et al. 2020). Research on OC preservation has traditionally focused on primary controls, such as high sedimentation rates and primary productivity (Keil 2017). Recent studies have questioned whether these factors influence the enrichment of OC in sediments (Keil and Cowie 1999; Kennedy et al. 2002; Crombez et al. 2017; Liu et al. 2018). Indeed, increasing attention is being paid to the mechanisms of OM preservation, in particular the protective sorption to mineral surfaces (Lalonde et al. 2012; Blattmann et al. 2019; Hemingway et al. 2019; Kleber et al. 2021).

Sediment grain size with different mineral surfaces can indirectly present physical protection for OM from attack by microorganisms along continental margins (Mayer 2004; Arndt et al. 2013; LaRowe et al. 2020). It is suggested that there is a strong relationship between sediment grain size and OC% due to the greater sorption capacity of fine sediments with large surface areas (Hedges and Keil 1995; Mayer 2004; Keil and Mayer 2014). In addition, sediment grain size not only has a potential impact on the dispersal and burial of OM along continental margins but also affects the veracity of

*Correspondence: baorui@ouc.edu.cn

Data Availability Statement: The data that supports the findings of this study are available in the Supporting Information of this article.
Associate editor: Xiao Hua Wang

organic signatures preserved in the deep-ocean sedimentary record (Inthorn et al. 2006; Ausín et al. 2021). This indicates that the size distribution of sediment is important for the study of OM preservation in sediments. Especially, most organic compounds are contrated in fine fraction which makes the examination of ultrafine particles very important (Kaiser and Guggenberger 2000; Benner and Amon 2015; Bu et al. 2017; Liu et al. 2018; Ge et al. 2020; Ausín et al. 2021). For instance, the presence of clay in ultrafine particles significantly affects the concentrations of OM (Blattmann et al. 2019).

Previous studies have used various techniques such as wet and/or dry sieving to separate particles in fine or large-grained sediments (Fox et al. 2017; Upadhayay et al. 2021). However, these methods are inadequate to effectively separating the ultrafine fraction ($< 10\,\mu$m) of marine sediment. Other methods have been employed; for example, SPLITT (Split Flow Thin Cell) fractionation or tube settling, but they either lack precise particle separation in size classes $< 10\,\mu$m or only sieve the $< 2\,\mu$m fraction (Coppola et al. 2005, 2007; Magill et al. 2018; Szparaga et al. 2018; Lattaud et al. 2022). These fractionation processes of grain size usually involve high sample amounts, low throughput, potential contamination, and loss of material to the separation medium, hindering our research on the synergistic effects of mineral matrix and OM in the ultrafine fractions of marine sediments.

Here, we develop an ultrafine particle separator (UPS) that allows us to fractionate the ultrafine particles from marine sediment. The UPS device is made up of a suspended particle generator (SPG) and a particle size separating device (PSSD), as shown in Fig. 1. The SPG concept was proposed by Amante-Orozco (2000) and Mendez et al. (2013) and has been commonly used in the production of dust or mineral aerosols (Gill et al. 2006; Domingo et al. 2010), and the PSSD was introduced by Furuuchi et al. (2010) for collecting aerosol particles of different sizes. In this study, we utilize the SPG to convert marine sediments into suspended particles; then these particles are collected and further sieved into different size ranges by using a PSSD. By combining SPG and PSSD, we develop a method to separate the ultrafine particles of marine sediments successfully based on the inertial impaction principle. Meanwhile, we evaluate the conversion performance, coupling effect, and sieving performance, respectively, of the designed and assembled device. In general, our study aims to develop a screening device for ultrafine particles in marine sediments and measure the OC contents and stable carbon isotope compositions of ultrafine fractions.

Materials and procedures

The inertial screening device mainly consists of a SPG and a PSSD (Fig. 1). The SPG is composed of three parts: (1) an ionizing blower, (2) a generating chamber, and (3) a collection chamber (Fig. 1a). The ionizing blower is used to eliminate electrostatic effects during SPG operation. The generating chamber can achieve the conversion of ultrafine particles to suspended particles, and the collecting chamber is utilized for collecting and concentrating suspended particles. The PSSD is a commercial product that is designed for partitioning the dust particles into eight different particle sizes: 0.43–0.65, 0.65–1.10, 1.10–2.10, 2.10–3.30, 3.30–4.7, 4.70–5.80, 5.80–9.00, and 9.00–10.00 μm. Here, we use the PSSD for sieving ultrafine suspended marine sediments into the eight fractions.

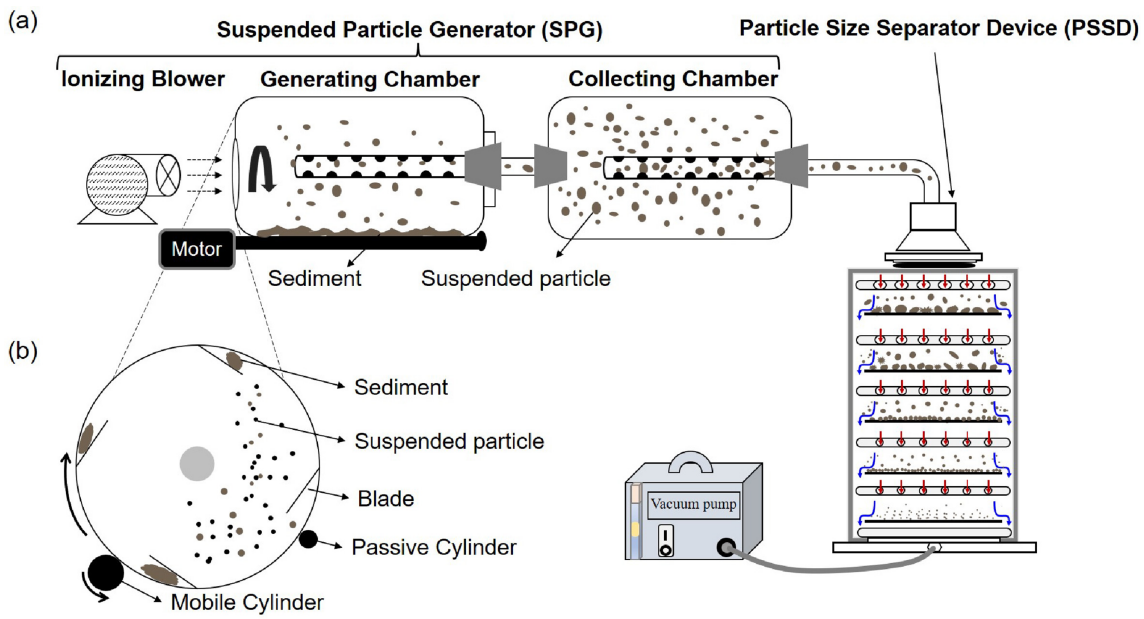


Fig. 1. (**a**) Schematic diagram of the UPS device: SPG and PSSD assembly. (**b**) Cross-section view of the generating chamber and moving parts.

15415856, 0, Downloaded from https://aslopubs.onlinelibrary.wiley.com/doi/10.1002/lom3.10676 by Rui Bao - Ocean University Of China , Wiley Online Library on [19/02/2025]. See the Terms and Conditions (https://onlinelibrary.wiley.com/terms-and-conditions) on Wiley Online Library for rules of use; OA articles are governed by the applicable Creative Commons License

Suspended particle generator description

A SPG has been built based on the design proposed by Amante-Orozco (2000) and Mendez et al. (2013) for a simple dust generator. In this study, the suspended particle generating chamber used is a PVC bottle measuring 125 mm wide and 240 mm tall. It contains four PVC blades (30 × 200 mm), which are positioned at a 30° angle to the surface of the bottle (Fig. 1b). These blades are responsible for mixing the sediment sample as the bottle rotates. Air with an opposite electric charge is introduced into the bottle through a 25 mm diameter orifice located at one end, while a 10 mm diameter PVC tube is inserted and secured to the cap at the other side. The tube inside the generating chamber is equipped with four rows of seven holes (2 mm diameter), spaced 12 mm apart along the tube. These holes are positioned perpendicular to each other. The portion of the tube outside the generating chamber is connected to the collection chamber. This arrangement allows the generating chamber to rotate while the collecting chamber remains stationary. The generating chamber is supported by two cylinders: a 300 mm long and 25 mm wide mobile one (connected to a small motor in this case) and a 300 mm long and 10 mm wide passive cylinder. The mobile cylinder is rotated at a speed of 60 rpm, resulting in a rotation speed of 5 rpm for the generating chamber.

The collecting chamber is a PVC bottle measuring 125 mm wide and 240 mm tall. Inside the chamber, a PVC tube with a diameter of 10 mm and a length of 100 mm is positioned perpendicular to the main axis of the chamber. There are four small holes in the circle of the tube and a series of four holes evenly distributed in the tube, each with a diameter of 2 mm. The tube connects the collecting chamber to a dust monitor (not shown in Fig. 1), which is used to track changes in the concentration of suspended particles within the chamber. On the opposite side of the suspended particle collecting chamber, another 10 mm diameter tube is inserted and securely attached to the cap. The portion of this tube inside the generating chamber has four rows of seven holes, each with a diameter of 2 mm. These rows are positioned perpendicular to each other on the tube. The section of the tube outside the collecting chamber is linked to the sampling port of PSSD. The vacuum pump provides a 15 L min^{-1} aspiration capacity for PSSD.

Suspended particle generator operation and calibration

The sediment is firstly sieved through a 20 μm diameter sieve to exclude large aggregates and ensure comparability among sediment particles (Wu et al. 2023). Once sieved, the sediment sample, weighing approximately 2 g, is transferred to the generating chamber, and other components including the ionizing blower, SPG, dust monitor, rotameter, and electric motor are activated sequentially. The generating chamber rotates and transports the sediment sample from bottom to up before it falls back down (Fig. 1a). During sediment falling, ultrafine particles in the sediment are converted to suspended particles. The airflow generated by the rotameter transports the suspended particles to the collecting chamber, where they are then captured by the dust monitor to measure the concentration of suspended particles. The dust monitor is calibrated to record the average concentration (expressed in mg m^{-3} of air) every 5 s.

In order to evaluate the stability and sensibility of SPG to the large sediments which might associate with a few ultrafine particles, we start to test suspended particle emissions of freeze-dried sediments (bulk, < 20, 20–63, and > 63 μm). The repeatability of the device is evaluated by measuring the suspended particles of each sediment three times, and the coefficient of variation between repetitions was calculated. Additionally, we analyze the suspended particle concentration with increasing time (emission curve); the average concentration throughout the experiment, the maximum concentration, and the total suspended particle emission (TSP) are also examined.

The TSP, expressed in milligrams of PM_{10} per gram of marine sediment: mg g^{-1}, is calculated by Eq. 1 (Mendez et al. 2013):

$$\mathrm{TSP} = \frac{\mathrm{PS_{ave}} \times \mathrm{Vol} \times \mathrm{DT}}{\mathrm{SW}} \quad (1)$$

where TSP is the total suspended particle emission in mg g^{-1} of sediment, PS_{ave} is the average suspended particle concentration along the experiment measured by the dust monitor in mg m^{-3} of air, Vol is the air volume removed by the rotameter in m^3 min^{-1}, DT is the experiment duration in min, and SW is the marine sediment sample weight.

Particle size separating device calibration standards

The PSSD is based on the inertial impact principle and operates at a volumetric flow rate of 15 L min^{-1}, after connection of the SPG. This PSSD consists of an impactor, a collection plate, and a flowmeter (Fig. 1a). The particles with sufficient inertia are impacted into the well upon a circular 80 mm diameter PTFE membrane filter in the collection plate immersed in 2 mL of distilled water. A water-immersed porous surface is selected for an impaction plate because of the ability of water to wick through previously deposited particulate and present a continuously wetted surface to the incoming suspended particle (Turner and Hering 1987; Le and Tsai 2021; Gong et al. 2023). However, the acquisition performance of the PSSD may be affected due to the connection of the SPG. Therefore, it is necessary to test and evaluate the acquisition efficiency of the PSSD after the connection of the SPG.

According to the penetrometry method, which is usually used to evaluate the accuracy of impactor properties (Peters et al. 2001), we test and evaluate the sieving performance of PSSD. First, we measured the number concentration of suspended particles collected from each level of collection plates in the PSSD by Particle Fallout Count and calculated the

15415856, 0, Downloaded from https://aslopubs.onlinelibrary.wiley.com/doi/10.1002/lom3.10676 by Rui Bao - Ocean University Of China , Wiley Online Library on [19/02/2025]. See the Terms and Conditions (https://onlinelibrary.wiley.com/terms-and-conditions) on Wiley Online Library for rules of use; OA articles are governed by the applicable Creative Commons License

acquisition efficiency of PSSD by Eq. 2 (Peters et al. 2001). The acquisition efficiency curve is then plotted based on the discrete particle size until a sufficient number of particle sizes have been evaluated to describe the Da_{50} value (50% of the particles below specific size in aerodynamic diameter penetrate to the sample collection filter) of the impactor.

$$\eta = 1 - \frac{C_2}{C_1} \times 100\% \quad (2)$$

where η is the acquisition efficiency of suspended particles. C_1 is the number of particles upstream of the separation, and C_2 is the number of particles downstream of the separation.

It should be noted that this method correctly accounts for partial impactor jet and interstage losses; thus, it is possible to describe the performance of the impactor precisely (Peters et al. 2001; Okuda et al. 2015). Furthermore, the accuracy of the sieving device is also tested and evaluated using a Malvern laser particle size analyzer and a scanning electron microscope (SEM).

Sample and pretreatment

Surface sediment has been collected from the East China Sea (ME3 28.73°N/122.58°E, LS02 27.85°N/125.4°E, P05 30.2°N/124.15°E), Yellow Sea (H01 35.96°N/121.01°E) and Bohai Sea (B18 38.01°N/119.78E) (Fig. 2). After freeze-drying the sediment sample, 1–2 g sediment is introduced to the generating chamber, and the components of the device are connected in a specific sequence (Fig. 1). Subsequently, the sediments divided into eight fractions by PSSD are collected and deposited on glass fiber filter.

After the freeze-dried fractionated sediments were weighed into Ag capsules, they were placed on a ceramic tray above a beaker filled with 37% HCl that was placed at the bottom of a desiccator. The desiccator was evacuated, and the samples were heated in an oven at 60°C for 72 h. After fumigation, excess acid was neutralized by replacement with ~20 g NaOH pellets in a pre-combusted Petri dish (60°C for 72 h, Bao et al. 2018). The concentrations of TOC and the $\delta^{13}C$ were measured using an EA-IsoLink elemental analyzer with a MAS 200R autosampler coupled to a MAT253 plus isotope ratio mass spectrometer via a ConFloIV universal interface (Thermo Fisher Scientific, Germany) at the Key Lab of Submarine Geosciences and Prospecting Techniques, Ministry of Education, Ocean University of China. The size accuracy of collected samples, measured values of OC concentration, and $\delta^{13}C$ in different grain sizes are listed in Table S1.

Assessment

Performance and sensitivity of suspended particle generator

The emission curve of suspended particles displayed similar patterns across sediment samples of different sizes (Fig. 3).

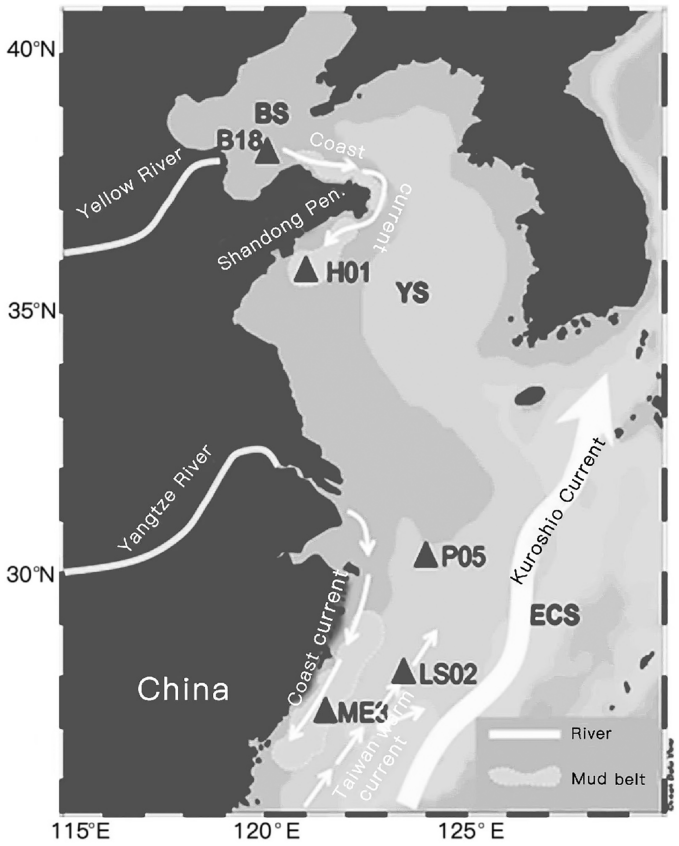


Fig. 2. Sample locations in Bohai Sea (BS), Yellow Sea (YS), and East China Sea (ECS). The arrows show the main marine currents and direction in the Chinese marginal sea.

Initially, there was a rapid linear increase in the concentration of suspended particles within the first 210 s until it peaked at the maximum concentration. Subsequently, the concentration decreased exponentially until it reached a constant level (stabilization zone). The curves generated using the SPG exhibited a time-dependent pattern that closely resembled previous findings reported by Gill et al. (2006) and Mendez et al. (2013). However, these studies primarily focused on the generation and analysis of fugitive suspended particles or compared the emission characteristics of suspended particles from surface soils. Therefore, this result confirms that successful transfer from marine sediments to suspended particles can be achieved using the SPG.

We conducted an analysis of the maximum, mean, and total concentrations of various suspended particles, along with calculating the coefficients of variation for mean concentrations (Table S2). The coefficient of variation for the mean concentration of suspended particles in all examined sediments ranges from 0.33 to 0.39, consistent with values reported in prior studies involving different types of dust generators (Amante-Orozco 2000; Wu et al. 2023). The elevated coefficient of variation values are primarily attributed to the variability in sediment composition or operational deficiencies in

15415856, 0, Downloaded from https://aslopubs.onlinelibrary.wiley.com/doi/10.1002/lom3.10676 by Rui Bao - Ocean University Of China , Wiley Online Library on [19/02/2025]. See the Terms and Conditions (https://onlinelibrary.wiley.com/terms-and-conditions) on Wiley Online Library for rules of use; OA articles are governed by the applicable Creative Commons License

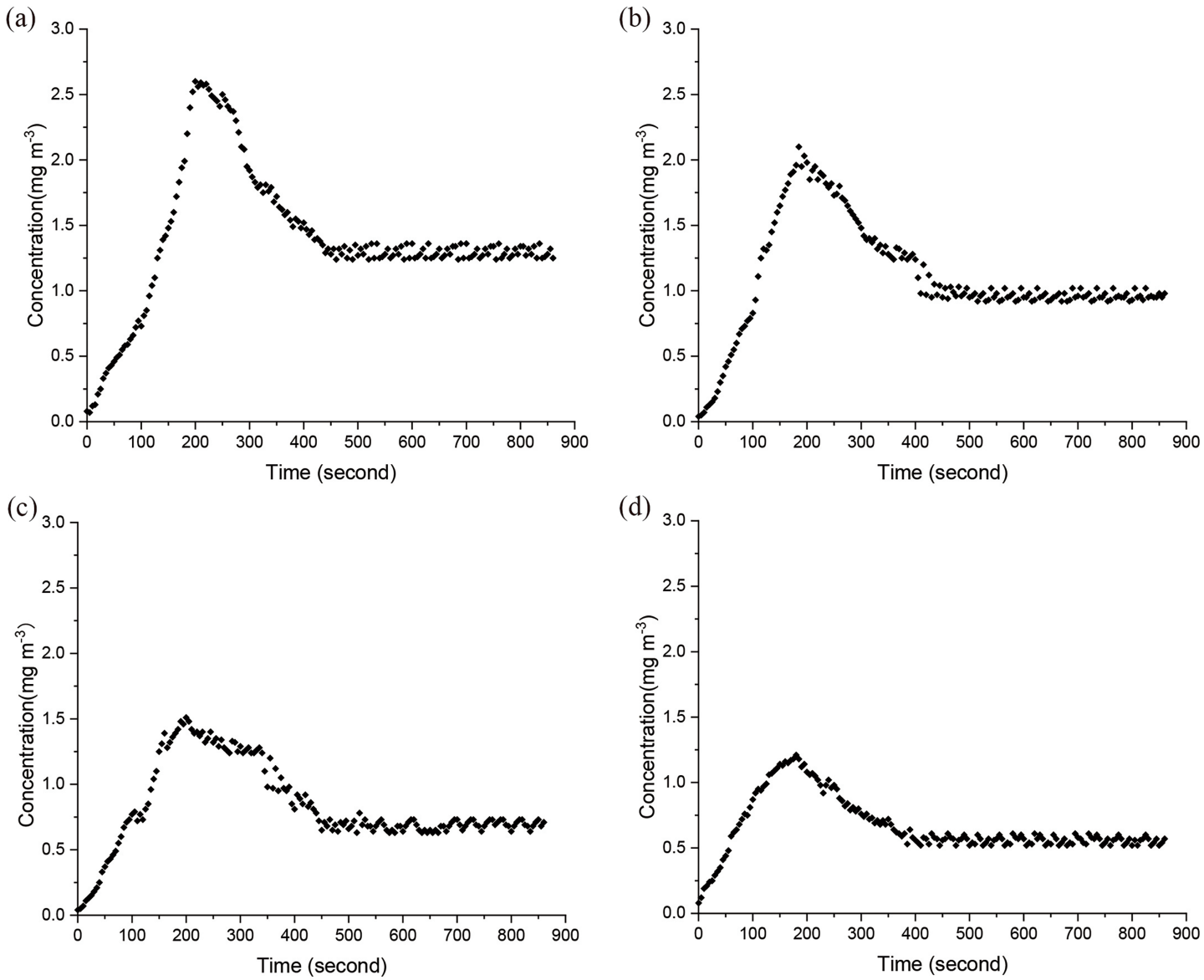


Fig. 3. Changes in suspended particle emission over time for different sediment sizes. (**a**) bulk sample after grinding, (**b**) < 20 μm, (**c**) 20–63 μm, and (**d**) > 63 μm samples.

the SPG, such as errors in sediment sample weighing, fluctuations in air flux rates, or variations in the rotation speed of the generator during measurements (Petit et al. 2021). This is corroborated by the coefficients of variation observed in our study, which align with those reported in previous research involving other types of dust generators (Amante-Orozco 2000; Wu et al. 2023).

Evaluation of particle size separating device acquisition efficiency

When evaluating PSSD, it is not always necessary to test a comprehensive efficiency curve that accounts for all particle sizes. Instead, the impactor in PSSD with a "steep cutoff" curve is considered the best choice as it closely approximates a step function efficiency curve (Peters et al. 2001; Patel and Aggarwal 2022). This design assumes that particles larger than a specific aerodynamic size are completely captured, while particles smaller than this size pass through the impactor. The Stokes number (Stk) is an important parameter for characterizing the efficiency of the impactor (Peters et al. 2001; Pui et al. 2014). Specifically, Stk_{50} represents the particle acquisition efficiency of 50%, and Da_{50} represents the corresponding impactor size.

The acquisition efficiency curve of the PSSD coupled to the SPG device was tested (Fig. 4). We select a reverse asymmetric sigmoid equation from multiple equations based on the sum of squares and correlation coefficient as our criteria for fit analysis. This equation (Peters et al. 2001) is expressed as

15415856, 0, Downloaded from https://aslopubs.onlinelibrary.wiley.com/doi/10.1002/lom3.10676 by Rui Bao - Ocean University Of China , Wiley Online Library on [19/02/2025]. See the Terms and Conditions (https://onlinelibrary.wiley.com/terms-and-conditions) on Wiley Online Library for rules of use; OA articles are governed by the applicable Creative Commons License

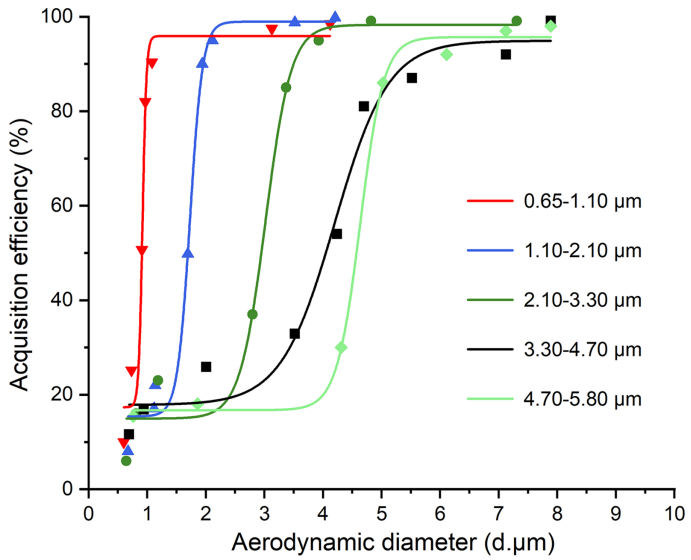


Fig. 4. Fitted acquisition efficiency curve for five each stage (0.65–1.10, 1.10–2.10, 2.10–3.30, 3.30–4.70, 4.70–5.80 μm).

$$y = 1 - a - b\left\{1 - \left[1 + \exp\left(\frac{x + d\ln\left(\sqrt[f]{2} - 1\right) - c}{d}\right)\right]^{-f}\right\} \quad (3)$$

where a, b, c, d, and f are curve parameters; x and y are the aerodynamic diameter and acquisition efficiency. Although simpler algorithms have been found to fit symmetrical acquisition efficiency curves adequately, they do not fit non-symmetrical performance curves as well as the function provided by the equation.

Based on the curve that best fits the experimental data, the final design of the PSSD has a Da_{50} cut-size of 4.750, 4.051, 2.911, 1.682, and 0.898 μm. These experimental findings are consistent with the theoretical cut-point of the PSSD as shown in Table S3. However, for 0.43–0.65 μm particles, we could not collect enough mass due to nanoscale size properties and relatively huge mass loss. Additionally, the 5.80–9.00 and 9.00–10.00 μm particles have the potential to disaggregate, which induces the inaccurate results. Therefore, the efficiency curves have not been tested for particle sizes ranging from 0.43–0.65, 5.80–9.00, and 9.00–10.00 μm. Nevertheless, the PSSD can achieve the desired outcomes by examining and interpreting the results of efficiency curves at all sampler levels.

Availability of the ultrafine particle separator device

To assess whether the UPS device can be available for the size sieving of marine ultrafine sediments, the collected suspended particles are tested using a Malvern Laser Particle Size Analyzer and SEM to measure the size and morphology. The results from the Malvern Laser Particle Size Analyzer confirmed that the particle size distribution of the sediment collected on the plate of the sieving device corresponded with the expected range, accounting for 86.7%, 92.0%, 93.9%, 85.2%, 78.4%, and 75% (red part in Fig. 5a–f). To account for particle agglomeration and the limitations of the Malvern Laser Particle Size Analyzer, the particle size distribution of the first and second levels was examined using SEM (Fig. S1). The SEM image shows that the particle size distribution is mainly distributed in 5.80–9.00 and 9.00–10.00 μm, with few particles outside this range. Overall, these results confirm that the designed UPS device possesses great accuracy in the sieving performance for ultrafine sediment.

To address the electrostatic interaction between suspended particles and the chamber walls, an ionizer blower has been incorporated into the device. This blower counteracts the electrostatic effect by introducing air with an opposing charge into the device. Furthermore, a mass recovery test using sediment samples was carried out. Due to the limitation of very few ultrafine particles in most sediments, there is not enough mass of ultrafine particles to calculate the recovery efficiency in each layer of the collection plate. Therefore, here we carried out an independent experiment to test the mass recovery of the UPS device. Specifically, we first fully milled bulk sediment to ensure that there are enough ultrafine particles. Then, we collected a sufficient amount of sediments in each range, and each layer of ultrafine particles was mixed with > 10 μm sediments to carry out a second screening separately, and the sediments in the corresponding range were collected finally. The recovery mass in each layer of the collection plate was calculated by Eq. 4:

$$R = \frac{m_{2nd}}{m_{1st}} \times 100\% \quad (4)$$

where R represents the mass recovery of the UPS device, m_{1st} represents the first collected mass of a certain range of grain size fraction, and m_{2nd} represents the second collected mass of a certain range of grain size fraction in the individual screening process.

To evaluate the reproducibility of the recovery rates associated with this method, we conducted identical experiments using two different fully milled sediment samples, both yielding comparable results. Table S4 presents mass recovery rates ranging from 77.7% to 88.7% at each stage of the screening unit, with an overall recovery rate of 84.2%. It is important to note that recovery rates for the 0.43–0.65 and 0.65–1.10 μm fractions could not be calculated due to the minimal mass collected; thus, we report the combined recovery for the two fractions (0.43–1.10 μm). The lowest recovery rates were observed in the size ranges of 0.43–1.10 and 1.10–2.10 μm. This may be attributed to the potential loss of ultrafine sediments during the sieving, collection, and elution processes, which can occur due to their high solubility and electrostatic interactions. These processes are likely to result in greater mass loss for finer particles compared to relatively coarser particles, which may

15415856, 0, Downloaded from https://aslopubs.onlinelibrary.wiley.com/doi/10.1002/lom3.10676 by Rui Bao - Ocean University Of China , Wiley Online Library on [19/02/2025]. See the Terms and Conditions (https://onlinelibrary.wiley.com/terms-and-conditions) on Wiley Online Library for rules of use; OA articles are governed by the applicable Creative Commons License

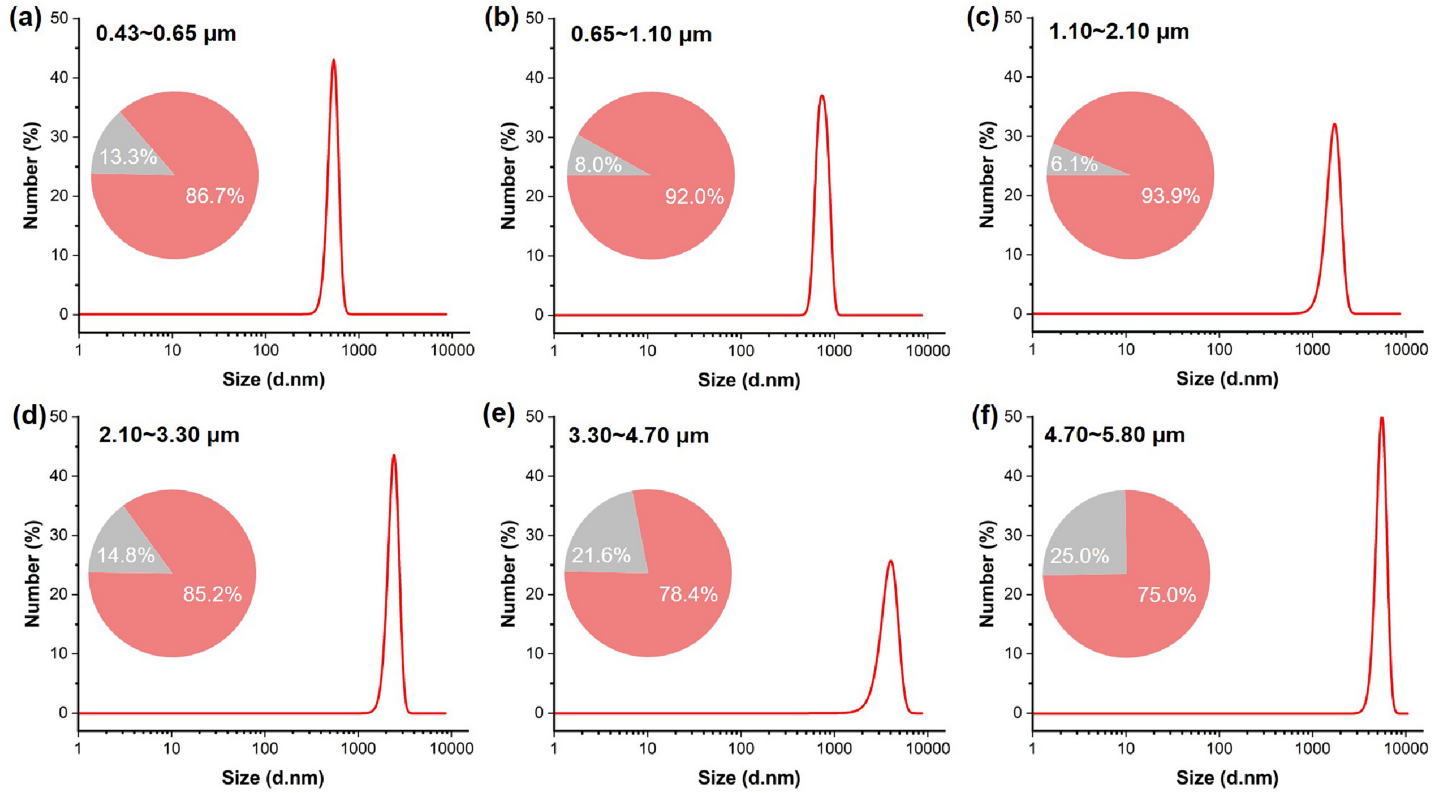


Fig. 5. Particle size distribution results of suspended particles from each level of the collection plate. (**a**–**f**) represent the particle size distributions of the first to sixth stage collection plates (0.43–0.65, 0.65–1.10, 1.10–2.10, 2.10–3.30, 3.30–4.70, 4.70–5.80 μm). In the pie chart, the red and gray parts indicate the proportions of the expected particle size ranges that correspond and do not correspond, respectively. Due to some aggregates within 5.80–9.00 and 9.00–10.00 μm particles may disaggregate in solution, we used Scan Electron Microscope (SEM) to observe the particle size distributions of these two fractions rather than Malvern Laser Particle Size Analyzer (Fig. S1).

influence the measurements of elemental content and isotopes across different grain-size groups. Our findings indicate that the mass recovery associated with the inertial sieving method is lower than that of other techniques, such as SPLITT fractionation, which has been reported to achieve recovery rates ranging from 80% to 97% (Coppola et al. 2007). However, we emphasize that the primary focus of the inertial sieving method is on particles smaller than 10 μm, and all mass recovery results pertain to various ultrafine particle sizes. In contrast, the mass recovery reported for SPLITT fractionation predominantly involves coarser particles. Therefore, we propose that the inertial sieving method may demonstrate superior performance specifically for the sieving of particles less than 10 μm.

The organic carbon characteristic in different sized ultrafine sediments

To reveal the grain size differences of sediment, the grain size distribution of ultrafine particles in five sites is shown in Fig. S2. We cannot obtain the bulk ultrafine particles; hence the percentage of < 10 μm was calibrated by measuring the grain size distribution of bulk sediments. These sediments have similar grain size distribution in ultrafine particles except for ME3, which has a higher percentage of 5–10 μm particles. Furthermore, we conducted the OC distribution among various size fractions of marine ultrafine particles. The results of OC content distribution in different size fractions of ultrafine particles are depicted in Fig. 6a. The OC content of ultrafine particles ranged from 1.894% to 5.916%, with a mean value of 3.478% ± 1.308% ($n = 7$) at site ME3, and from 1.995% to 2.802%, with a mean value of 2.327% ± 0.305% ($n = 6$) at site LS02. These OC content values are notably higher than the mean OC value in bulk sediments found in offshore sediment (0.5% ± 0.3, $n = 240$) (Bao et al. 2016). It is evident that ultrafine sediments contain superior OC content and increases as the particle size decreases in all five samples.

The OC content demonstrates a consistent pattern in ultrafine particles from the China Marginal Sea. The clay fraction (< 2.10 μm) exhibits the highest OC content, while the silt fraction (2.10–10.0 μm) shows consistent peaks in the 4.70–5.80 μm fractions, with additional peaks observed in the 9.00–10.00 μm fractions (Fig. 6a). This trend aligns with previous studies, underscoring the significance of studying ultrafine particles in biogeochemical research. We think that the inertial sieving device technique offers a promising method to analyze the mineral and OC content in sediments

15415856, 0, Downloaded from https://aslopubs.onlinelibrary.wiley.com/doi/10.1002/lom3.10676 by Rui Bao - Ocean University Of China , Wiley Online Library on [19/02/2025]. See the Terms and Conditions (https://onlinelibrary.wiley.com/terms-and-conditions) on Wiley Online Library for rules of use; OA articles are governed by the applicable Creative Commons License

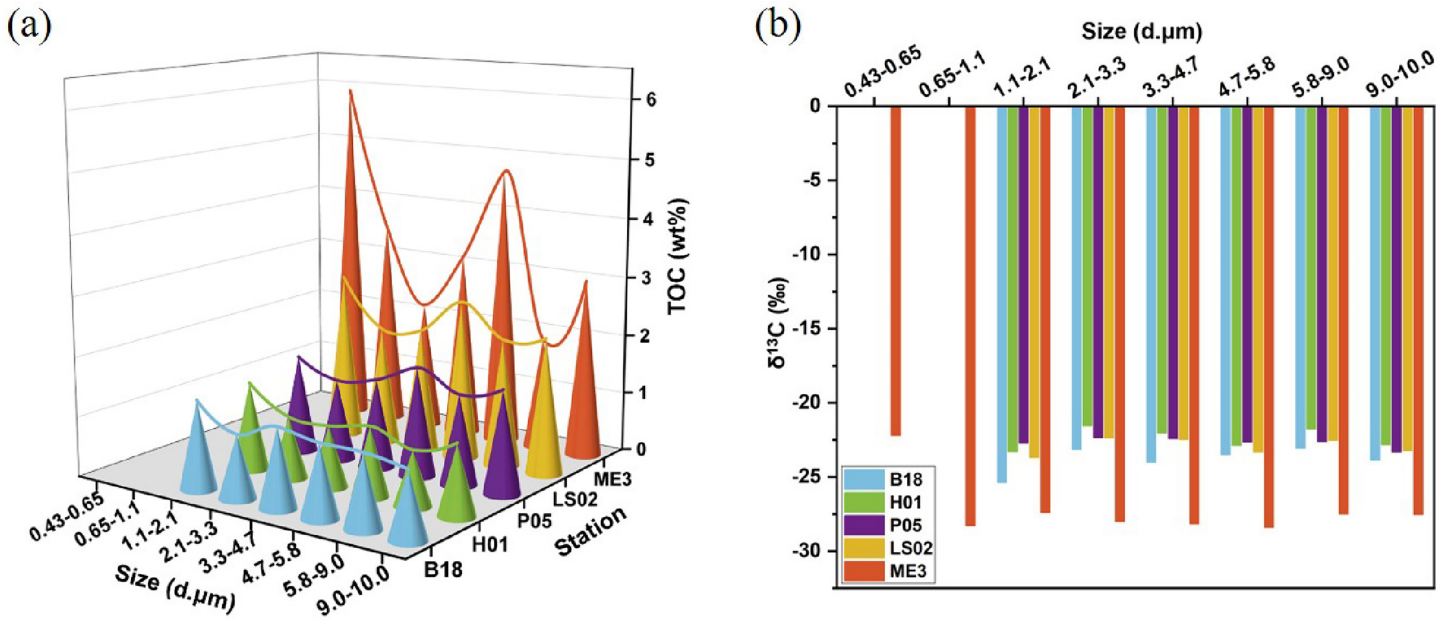


Fig. 6. Distribution of parameters for different particle size components. (**a**) OC content (OC%) and (**b**) $\delta^{13}C$ (‰) values. Organic carbon and $\delta^{13}C$ values were not determined for the 0.43–0.65 and 0.65–1.10 μm fractions due to the collected mass being very little, resulting in OC content below the instrumental detection limit.

(Mayer 2004; Gu et al. 2023) and investigate the impact of grain size on OC preservation (Bergamaschi et al. 1997; Bianchi et al. 2018; Tesi et al. 2014).

The $\delta^{13}C$ distributions of OC in ultrafine particles from the East China Sea (ME3, LS02, and P05), Yellow Sea (H01), and Bohai Sea (B18) are illustrated in Fig. 6b. The $\delta^{13}C$ values of ultrafine particulate organic carbon in ME3 range from −28.49‰ to −22.33‰, with a mean value of −27.10‰ ± 1.82‰ ($n = 8$). For P05, the range is from −23.33‰ to −22.35‰ with a mean value of −22.68‰ ± 0.32‰ ($n = 6$); H01 ranges from −23.31‰ to −21.55‰ with a mean value of −22.40‰ ± 0.64‰ ($n = 6$); LS02 ranges from −23.70‰ to −22.37‰ with a mean value of −22.93‰ ± 0.50‰ ($n = 6$); and B18 ranges from −25.37‰ to −23.06‰ with a mean of −23.82‰ ± 0.77‰ ($n = 6$). The $\delta^{13}C$ values of ME3 show large variation among these results, and there is a relatively homogeneous $\delta^{13}C$ value (−28.49‰ to −27.40‰) in 0.65–10 μm fractions. The relatively negative $\delta^{13}C$ value (−22.33‰) of 0.43–0.65 μm fractions is a critical factor in vary largely of $\delta^{13}C$ value in ME3, which may be induced by the contribution of more marine OC source (Ogrinc et al. 2005; Megens et al. 2002).

The presence of land-sourced C_4 plant organic matter may lead to an underestimation of the relative contribution of terrestrial source organic carbon in ultrafine particles at station H01 in the Yellow Sea. Terrestrial organic matter transported by rivers plays a significant role in the organic matter content of ultrafine particles at site B18 in the Bohai Sea. Comparison of $\delta^{13}C$ results from ME3, P05, and LS02 in the East China Sea indicates that the contribution of terrestrial sources accounts for a higher proportion of sediment ultrafine particles in the estuarine zone, while marine source organic matter contributes more to ultrafine particles in the middle and outer shelf.

Discussion

In this study, the UPS device was developed by integrating a PSSD with a SPG. Our device is capable of converting sediment into suspended particles, effectively separating them into ultrafine fractions. Notably, the UPS device used in this research only requires around 2 g of sediment sample, overcoming the challenge of handling large sediment samples associated with conventional screening methods. It is important to highlight that the sieving process resulted in very few collected particles in the size ranges of 0.43–0.65 and 0.65–1.10 μm due to electrostatic interactions between particles. Despite the introduction of an ionizing blower to the sieving device in an attempt to mitigate these effects, some limitations still persist. Therefore, further optimization of the screening device is necessary to improve the efficiency of particle acquisition at each stage.

The performance and efficiency of the two key components of the instrument (SPG and PSSD) were evaluated separately. In the SPG component, particles are generated in the generating chamber and then transferred to the collecting chamber for accumulation and concentration. The suspended particle emission curves consistently demonstrate a pattern where particle concentration rapidly increases until reaching a

15415856, 0, Downloaded from https://aslopubs.onlinelibrary.wiley.com/doi/10.1002/lom3.10676 by Rui Bao - Ocean University Of China , Wiley Online Library on [19/02/2025]. See the Terms and Conditions (https://onlinelibrary.wiley.com/terms-and-conditions) on Wiley Online Library for rules of use; OA articles are governed by the applicable Creative Commons License

maximum level, followed by a decrease towards a stable concentration (Fig. 3). When the concentration in the collecting chamber peaks, excess particles are transferred to the PSSD via a pipeline. Analysis of average particle concentrations and total emissions indicates the highest and lowest values in the bulk and > 63 μm fractions. This suggests that sediments of varying grain sizes can adsorb fine or ultrafine particles to form non-erodible aggregates under natural conditions. However, mechanical disturbances may lead to the emission of ultrafine particles (Madden et al. 2010).

Regarding the PSSD, the acquisition efficiency curve effectively represents its sieving performance. Figure 4 illustrates a steep acquisition curve for all levels, indicating excellent particle acquisition performance across the board. Nevertheless, some large and small particles are inevitably retained in the device. Despite this, the overall acquisition efficiency curve closely approaches the desired ideal, signifying the accuracy of the PSSD.

Further experiments were conducted to assess the practical application of the UPS device. Sediment samples were collected from the China marginal sea to sieve ultrafine particles using this device in this study. These ultrafine particles exhibited OC content ranging from 1.89% to 5.92%, which is higher than other sizes previously reported (Bao et al. 2016). The fine fraction plays a significant role in slope sediments and basin areas, contributing to 85% of TOC accumulation in the latter (Coppola et al. 2007). These results underscore the importance of understanding the characteristics and dynamics of ultrafine particles in sedimentary carbon preservation. The $\delta^{13}C$ values of the ME3 samples resembled those of modern soils from the Changjiang River, suggesting a predominant C_3 plant source (Liu et al. 2018). However, at station H01 in the Yellow Sea, the land-derived C_4 plants may constitute the terrestrial OC sources that contribute to the OC content of ultrafine particles. Terrestrial organic matter transported by rivers serves as a significant source of organic matter in ultrafine particles in the Bohai Sea. Comparison of $\delta^{13}C$ values between ME3, P05, and LS02 in the East China Sea revealed a predominant terrestrial source input of ultrafine particles in the estuarine zone, while marine source organic matter contributes more to ultrafine particles in the middle and outer shelf zones.

In general, effectively sieving and analyzing components of ultrafine particles in sediments pose challenges in preventing sample damage or contamination. Previous methods such as washing (Liu et al. 2013) have been abandoned due to their adverse effects. The SPLITT method and other techniques have limitations (Table S5) that hinder the screening of ultrafine particle fractions without loss or contamination. Thus, the UPS device developed in this study fulfills the sieving requirements for ultrafine particles effectively.

Comments and recommendations

Due to the unique viscosity of ultrafine particles and the limitations of traditional screening methods, further sieving of ultrafine sediments into finer particles presents significant challenges. In this study, we present the development of UPS, which is based on the inertial sieving method commonly employed in aerosol separation devices used in atmospheric science. The UPS is capable of finely separating ultrafine particles from sediments with grain sizes less than 10 μm, facilitating the exploration of the organic geochemical characteristics of organic carbon in ultrafine particles across various grain sizes. This advancement offers important methodological support for investigating the marine organic carbon cycle at the nanoscale. However, several limitations persist, as the UPS is unable to collect sufficient sample mass of extremely fine particles (0.43–0.65 and 0.65–1.10 μm) in this case. This indicates that the method is particularly advantageous for screening sediments with a higher content of ultrafine particles. In conclusion, the ultrafine particle screening device can accurately perform multi-stage fine screening of ultrafine particles, providing individual insights into the composition of ultrafine particles in marine sediments, especially in the context of studying the OC cycle within these particles. Additionally, the device is cost-effective to manufacture and easy to install, making it an accessible tool for enhancing our understanding of the organic geochemical information contained within the ultrafine particulate components of marine sediment.

Author Contributions

The first three authors are joint first authors. Guangjin Zhen carried out the analyses and wrote analyses and wrote the orignal draft. Mengyao shen and Nan Wang discussed the results and reviwed the manuscript. YangLi Che, Haoshuai Li and Caiqing Yan provided the samples and curated the data. Rui bao conceptualized the research and acquired funding.

Acknowledgments

This manuscript is a contribution of the National Natural Science Foundation of China (42450135, 92058207 and 42076037), the Fundamental Research Funds for the Cebtral Universities (202042010), Taishan Young Scholars (tsqn202103030), and Shandong Province Natural Science Foundation (ZR2021JQ12).

Conflicts of Interest

None declared.

References

Amante-Orozco, A. 2000. Fine Particulate Matter Generation Under Controlled Laboratory and Wind Tunnel Conditions. Lubbock: Texas Tech University.

Arnarson, T. S., and R. G. Keil. 2007. "Changes in OM–Mineral Interactions for Marine Sediments With Varying Oxygen Exposure Times." *Geochimica et Cosmochimica Acta* 71: 3545–3556. https://doi.org/10.1016/j.gca.2007.04.027.

15415856, 0, Downloaded from https://aslopubs.onlinelibrary.wiley.com/doi/10.1002/lom3.10676 by Rui Bao - Ocean University Of China , Wiley Online Library on [19/02/2025]. See the Terms and Conditions (https://onlinelibrary.wiley.com/terms-and-conditions) on Wiley Online Library for rules of use; OA articles are governed by the applicable Creative Commons License

Arndt, S., B. B. Jørgensen, D. E. LaRowe, J. J. Middelburg, R. D. Pancost, and P. Regnier. 2013. "Quantifying the Degradation of OM in Marine Sediments: A Review and Synthesis." *Earth-Science Reviews* 123: 53–86. https://doi.org/10.1016/j.earscirev.2013.02.008.

Ausín, B., E. Bruni, N. Haghipour, C. Welte, S. M. Bernasconi, and T. I. Eglinton. 2021. "Controls on the Abundance, Provenance and Age of Organic Carbon Buried in Continental Margin Sediments." *Earth and Planetary Science Letters* 558: 116759. https://doi.org/10.1016/j.epsl.2021.116759.

Bao, R., C. McIntyre, M. Zhao, C. Zhu, S. J. Kao, and T. I. Eglinton. 2016. "Widespread Dispersal and Aging of Organic Carbon in Shallow Marginal Seas." *Geology* 44: 791–794. https://doi.org/10.1130/g37948.1.

Bao, R., T. S. van der Voort, M. Zhao, et al. 2018. "Influence of Hydrodynamic Processes on the Fate of Sedimentary OM on Continental Margins." *Global Biogeochemical Cycles* 32: 1420–1432. https://doi.org/10.1029/2018gb005921.

Benner, R., and R. M. W. Amon. 2015. "The Size-Reactivity Continuum of Major Bioelements in the Ocean." *Annual Review of Marine Science* 7: 185–205. https://doi.org/10.1146/annurev-marine-010213–135126.

Bergamaschi, B. A., E. Tsamakis, R. G. Keil, T. I. Eglinton, D. B. Montluçon, and J. I. Hedges. 1997. "The Effect of Grain Size and Surface Area on OM, Lignin and Carbohydrate Concentration, and Molecular Compositions in Peru Margin Sediments." *Geochimica et Cosmochimica Acta* 61: 1247–1260. https://doi.org/10.1016/s0016-7037(96)00394-8.

Bianchi, T. S., X. Cui, N. E. Blair, D. J. Burdige, T. I. Eglinton, and V. Galy. 2018. "Centers of Organic Carbon Burial and Oxidation at the Land–Ocean Interface." *Organic Geochemistry* 115: 138–155. https://doi.org/10.1016/j.orggeochem.2017.09.008.

Blattmann, T. M., Z. Liu, Y. Zhang, et al. 2019. "Mineralogical Control on the Fate of Continentally Derived OM in the Ocean." *Science* 366: 742–745. https://doi.org/10.1126/science.aax5345.

Bu, H., P. Yuan, H. Liu, et al. 2017. "Effects of Complexation Between OM (OM) and Clay Mineral on OM Pyrolysis." *Geochimica et Cosmochimica Acta* 212: 1–15. https://doi.org/10.1016/j.gca.2017.04.045.

Coppola, L., Ö. Gustafsson, P. Andersson, and P. Axelsson. 2005. "Fractionation of Surface Sediment Fines Based on a Coupled Sieve–SPLITT (Split Flow Thin Cell) Method." *Water Research* 39: 1935–1945. https://doi.org/10.1016/j.watres.2005.04.005.

Coppola, L., Ö. Gustafsson, P. Andersson, T. I. Eglinton, M. Uchida, and A. F. Dickens. 2007. "The Importance of Ultrafine Particles as a Control on the Distribution of Organic Carbon in Washington Margin and Cascadia Basin Sediments." *Chemical Geology* 243: 142–156. https://doi.org/10.1016/j.chemgeo.2007.05.020.

Crombez, V., F. Baudin, S. Rohais, et al. 2017. "Basin Scale Distribution of OM in Marine Fine-Grained Sedimentary Rocks: Insight From Sequence Stratigraphy and Multi-Proxies Analysis in the Montney and Doig Formations." *Marine and Petroleum Geology* 83: 382–401. https://doi.org/10.1016/j.marpetgeo.2016.10.013.

Domingo, R. A., R. J. Southard, and K. Lee. 2010. "Laboratory System for Dust Generation From Soils." *Journal of Environmental Quality* 39: 1254–1261. https://doi.org/10.2134/jeq2008.0380.

Fox, P. M., P. S. Nico, M. M. Tfaily, K. Heckman, and J. A. Davis. 2017. "Characterization of Natural OM in Low-Carbon Sediments: Extraction and Analytical Approaches." *Organic Geochemistry* 114: 12–22. https://doi.org/10.1016/j.orggeochem.2017.08.009.

Furuuchi, M., K. Eryu, M. Nagura, et al. 2010. "Development and Performance Evaluation of Air Sampler With Inertial Filter for Nanoparticle Sampling." *Aerosol and Air Quality Research* 10: 185–192. https://doi.org/10.4209/aaqr.2009.11.0070.

Ge, T., Y. Xue, X. Jiang, L. Zou, and X. Wang. 2020. "Sources and Radiocarbon Ages of Organic Carbon in Different Grain Size Fractions of Yellow River-Transported Particles and Coastal Sediments." *Chemical Geology* 534: 119452. https://doi.org/10.1016/j.chemgeo.2019.119452.

Gill, T. E., T. M. Zobeck, and J. E. Stout. 2006. "Technologies for Laboratory Generation of Dust From Geological Materials." *Journal of Hazardous Materials* 132: 1–13. https://doi.org/10.1016/j.jhazmat.2005.11.083.

Gong, W.-C., N. Jidenko, Y.-R. Li, T.-C. Le, J.-P. Borra, and C.-J. Tsai. 2023. "$PM_{0.1}$ Non-bouncing Impactor (NBI) for Ultrafine Particle Mass and Number Measurements." *Journal of Aerosol Science* 174: 106249. https://doi.org/10.1016/j.jaerosci.2023.106249.

Gu, Y., Q. Wan, X. Li, T. Han, S. Yang, and Q. Hu. 2023. "Structure and Evolution of Clay–Organic Nanocomposites in Three Leading Shales in China." *Journal of Earth Science* 34: 824–837. https://doi.org/10.1007/s12583-022-1717-y.

Hedges, J. I., and R. G. J. M. c. Keil. 1995. "Sedimentary OM Preservation: An Assessment and Speculative Synthesis." *Marine Chemistry* 49: 81–115. https://doi.org/10.1016/0304-4203(95)00008-f.

Hemingway, J. D., D. H. Rothman, K. E. Grant, et al. 2019. "Mineral Protection Regulates Long-Term Global Preservation of Natural Organic Carbon." *Nature* 570: 228–231. https://doi.org/10.1038/s41586-019-1280-6.

Inthorn, M., T. Wagner, G. Scheeder, and M. Zabel. 2006. "Lateral Transport Controls Distribution, Quality, and Burial of OM along Continental Slopes in High-Productivity Areas." *Geology* 34: 205–208. https://doi.org/10.1130/g22153.1.

Kaiser, K., and G. J. O. g. Guggenberger. 2000. "The Role of DOM Sorption to Mineral Surfaces in the Preservation of OM in Soils." *Journal of Organic Chemistry* 31: 711–725. https://doi.org/10.1016/S0146-6380(00)00046-2.

15415856, 0, Downloaded from https://aslopubs.onlinelibrary.wiley.com/doi/10.1002/lom3.10676 by Rui Bao - Ocean University Of China , Wiley Online Library on [19/02/2025]. See the Terms and Conditions (https://onlinelibrary.wiley.com/terms-and-conditions) on Wiley Online Library for rules of use; OA articles are governed by the applicable Creative Commons License

Keil, R. 2017. "Anthropogenic Forcing of Carbonate and Organic Carbon Preservation in Marine Sediments." *Annual Review of Marine Science* 9: 151–172. https://doi.org/10.1146/annurev-marine-010816-060724.

Keil, R. G., and G. L. J. M. G. Cowie. 1999. "OM Preservation Through the Oxygen-Deficient Zone of the NE Arabian Sea as Discerned by Organic Carbon: Mineral Surface Area Ratios." *Marine Geology* 161: 13–22. https://doi.org/10.1016/S0025-3227(99)00052-3.

Keil, R. G., and L. M. Mayer. 2014. "Mineral Matrices and OM." *Treatise on Geochemistry* 12: 337–359. https://doi.org/10.1016/b978-0-08-095975-7.01024-x.

Kennedy, M. J., D. R. Pevear, and R. J. J. S. Hill. 2002. "Mineral Surface Control of Organic Carbon in Black Shale." *Science* 295: 657–660. https://doi.org/10.1126/science.1066611.

Kleber, M., I. C. Bourg, E. K. Coward, C. M. Hansel, S. C. B. Myneni, and N. Nunan. 2021. "Dynamic Interactions at the Mineral–OM Interface." *Nature Reviews Earth and Environment* 2: 402–421. https://doi.org/10.1038/s43017-021-00162-y.

Lalonde, K., A. Mucci, A. Ouellet, and Y. Gélinas. 2012. "Preservation of OM in Sediments Promoted by Iron." *Nature* 483: 198–200. https://doi.org/10.1038/nature10855.

LaRowe, D. E., S. Arndt, J. A. Bradley, et al. 2020. "The Fate of Organic Carbon in Marine Sediments—New Insights From Recent Data and Analysis." *Earth-Science Reviews* 204: 103146. https://doi.org/10.1016/j.earscirev.2020.103146.

Lattaud, J., T. I. Eglinton, M. Tallon, L. Bröder, Z. Erdem, and B. Ausín. 2022. "Grain Size Controls on Long-Chain Diol Distributions and Proxy Signals in Marine Sediments." *Frontiers in Marine Science* 9: 1004096. https://doi.org/10.3389/fmars.2022.1004096.

Le, T.-C., and C.-J. Tsai. 2021. "Inertial Impaction Technique for the Classification of Particulate Matters and Nanoparticles: A Review." *KONA Powder and Particle Journal* 38: 42–63. https://doi.org/10.14356/kona.2021004.

Liu, H., P. Yuan, D. Liu, et al. 2018. "Pyrolysis Behaviors of OM (OM) With the Same Alkyl Main Chain but Different Functional Groups in the Presence of Clay Minerals." *Applied Clay Science* 153: 205–216. https://doi.org/10.1016/j.clay.2017.12.028.

Liu, Z., D. Breecker, L. M. Mayer, and J. Zhong. 2013. "Composition of Size-Fractioned Sedimentary OM in Coastal Environments Is Affected by Difference in Physical Forcing Strength." *Organic Geochemistry* 60: 20–32. https://doi.org/10.1016/j.orggeochem.2013.04.009.

Madden, N. M., R. J. Southard, and J. P. Mitchell. 2010. "Soil Water and Particle Size Distribution Influence Laboratory-Generated PM_{10}." *Atmospheric Environment* 44: 745–752. https://doi.org/10.1016/j.atmosenv.2009.11.044.

Magill, C. R., B. Ausín, P. Wenk, et al. 2018. "Transient Hydrodynamic Effects Influence Organic Carbon Signatures in Marine Sediments." *Nature Communications* 9: 4690. https://doi.org/10.1038/s41467-018-06973-w.

Mayer, L. M. 2004. "The Inertness of Being Organic." *Marine Chemistry* 92: 135–140. https://doi.org/10.1016/j.marchem.2004.06.022.

Megens, L., J. Van der Plicht, J. W. De Leeuw, and F. Smedes. 2002. "Stable Carbon and Radiocarbon Isotope Compositions of Particle Size Fractions to Determine Origins of Sedimentary OM in an Estuary." *Organic Geochemistry* 33: 945–952. https://doi.org/10.1016/S0146-6380(02)00060-8.

Mendez, M. J., J. E. Panebianco, and D. E. Buschiazzo. 2013. "A New Dust Generator for Laboratory Dust Emission Studies." *Aeolian Research* 8: 59–64. https://doi.org/10.1016/j.aeolia.2012.10.007.

Ogrinc, N., G. Fontolan, J. Faganeli, and S. Covelli. 2005. "Carbon and Nitrogen Isotope Compositions of OM in Coastal Marine Sediments (the Gulf of Trieste, N Adriatic Sea): Indicators of Sources and Preservation." *Marine Chemistry* 95: 163–181. https://doi.org/10.1016/j.marchem.2004.09.003.

Okuda, T., R. Isobe, Y. Nagai, S. Okahisa, K. Funato, and K. Inoue. 2015. "Development of a High-Volume $PM_{2.5}$ Particle Sampler Using Impactor and Cyclone Techniques." *Aerosol and Air Quality Research* 15: 759–767. https://doi.org/10.4209/aaqr.2014.09.0194.

Patel, P., and S. G. Aggarwal. 2022. "On the Techniques and Standards of Particulate Matter Sampling." *Journal of the Air & Waste Management Association (1995)* 72: 791–814. https://doi.org/10.1080/10962247.2022.2048129.

Peters, T. M., R. W. Vanderpool, and R. W. Wiener. 2001. "Design and Calibration of the EPA PM2.5 Well Impactor Ninety-Six (WINS)." *Aerosol Science and Technology* 34: 389–397. https://doi.org/10.1080/02786820120352.

Petit, H. A., C. I. Paulo, O. A. Cabrera, and E. F. Irassar. 2021. "Evaluation of the Dustiness of Fugitive Dust Sources Using Gravitational Drop Tests." *Aeolian Research* 52: 100724. https://doi.org/10.1016/j.aeolia.2021.100724.

Pui, D. Y. H., S.-C. Chen, and Z. Zuo. 2014. "$PM_{2.5}$ in China: Measurements, Sources, Visibility and Health Effects, and Mitigation." *Particuology* 13: 1–26. https://doi.org/10.1016/j.partic.2013.11.001.

Szparaga, A., T. Kowalkowski, and B. Buszewski. 2018. "Mathematical Modeling of Full Feed Depletion Split-Flow Lateral-Transport Thin Self-Adjustable Channels (FFD-SPLITT-SA)." *Journal of Chromatography. A* 1552: 67–72. https://doi.org/10.1016/j.chroma.2018.03.045.

Tesi, T., I. Semiletov, G. Hugelius, O. Dudarev, P. Kuhry, and Ö. Gustafsson. 2014. "Composition and Fate of Terrigenous OM along the Arctic Land–Ocean Continuum in East Siberia: Insights From Biomarkers and Carbon Isotopes." *Geochimica et Cosmochimica Acta* 133: 235–256. https://doi.org/10.1016/j.gca.2014.02.045.

Turner, J. R., and S. V. J. J. o. A. S. Hering. 1987. "Greased and Oiled Substrates as Bounce-Free Impaction Surfaces." *Journal*

15415856, 0, Downloaded from https://aslopubs.onlinelibrary.wiley.com/doi/10.1002/lom3.10676 by Rui Bao - Ocean University Of China , Wiley Online Library on [19/02/2025]. See the Terms and Conditions (https://onlinelibrary.wiley.com/terms-and-conditions) on Wiley Online Library for rules of use; OA articles are governed by the applicable Creative Commons License

of Aerosol Science 18: 215–224. https://doi.org/10.1016/0021-8502(87)90057-7.

Upadhayay, H. R., S. J. Granger, and A. L. Collins. 2021. "Dynamics of Fluvial Hydro-Sedimentological, Nutrient, Particulate OM and Effective Particle Size Responses During the U.K. Extreme Wet Winter of 2019–2020." *Science of the Total Environment* 774: 145722. https://doi.org/10.1016/j.scitotenv.2021.145722.

Wu, F., N. Song, T. Hu, S. S. H. Ho, J. Cao, and D. Zhang. 2023. "Surrogate Atmospheric Dust Particles Generated From Dune Soils in Laboratory: Comparison With Field Measurement." *Particuology* 72: 29–36. https://doi.org/10.1016/j.partic.2022.02.007.

Supporting Information

Additional Supporting Information may be found in the online version of this article.

Submitted 11 June 2024
Revised 25 November 2024
Accepted 06 February 2025

15415856, 0, Downloaded from https://aslopubs.onlinelibrary.wiley.com/doi/10.1002/lom3.10676 by Rui Bao - Ocean University Of China , Wiley Online Library on [19/02/2025]. See the Terms and Conditions (https://onlinelibrary.wiley.com/terms-and-conditions) on Wiley Online Library for rules of use; OA articles are governed by the applicable Creative Commons License